Ocean Engineering 223 (2021) 108631

Contents lists available at ScienceDirect

Ocean Engineering

journal homepage: www.elsevier.com/locate/oceaneng

Dynamic characteristics and responses of flow-conveying flexible pipe under consideration of axially-varying tension

Dingbang Yan [a,d,1], Shuangxi Guo [a,d,1], Yilun Li [b], Jixiang Song [a,d], Min Li [c], Weimin Chen [a,d,*]

[a] Institute of Mechanics, Chinese Academy of Sciences, Beijing, 100190, China
[b] Lab. MSSMat, CentraleSupélec, Université de Paris-Saclay, Gif sur Yvette, 91190, France
[c] School of Aeronautics Sciences and Engineering, Beihang University, Beijing, 100191, China
[d] University of Chinese Academy of Sciences,Beijing, 100049, China

ARTICLE INFO

Keywords:
Fluid-conveying pipe
Axially-varying tension
Dynamic characteristics and response
Fluid-solid coupling
WKB

ABSTRACT

As oil and gas industry is developing towards deeper ocean area, the length and flexibility of ocean pipes become larger, which may induce larger-amplitude displacement of flexible pipe response due to lower structural stiffness against environmental and operational loads. Moreover, these pipes also convey internal flow. In other words, the dynamic characteristics and response of the flow-conveying pipe face great challenge, such as bucking and flutter.

In this study, the dynamic characteristics and response of a flexible pipe, under internal flow and, particularly, axially-varying tension, are examined through our FEM numerical simulations. First, the governing equations and FEM models of a flexible pipe with axially-varying tension and internal flow are developed. Then the dynamic characteristics, including the coupled frequency and modal shape, are presented. At last, the dynamic response and corresponding stability behaviors are discussed and compared with the cases of pipe with uniform tension. Our FEM results show that the stability and response are quite different from pipe with uniform tension. And, the time-spatial evolution of pipe displacement exhibits a profound wave propagation effect, e.g. the wave length and peak value/position significantly change along structural length and the mechanism is discussed based on the WKB solutions.

1. Introduction

The pipes with internal flow were widely used in marine engineering, nuclear industry and oil exploitation. The dynamics of them is a typical fluid-solid coupling issue. The stability and response of them principally depends on the properties of internal flow and pipe structure, such as internal flow velocity, structural bending stiffness, axial tension and mass density. By now, there have been a large number of studies on the stability issue of the pipes with internal flow (Bourrières et al., 1939; Benjamin, 1961; Holmes, 1978; Gregory and Païdoussis, 1966a, 1966b), where the structural parameters are mostly uniform distributing along pipe length, or pipe tension keeps axially-constant. However, for a flexible pipe in deep water, the influence of the structural weight could not be negligible with the increasing structural length. Therefore, structure parameter, e.g. axial tension, would be no longer uniform along axial length. We may say that it is more challenging to study the stability and even dynamic response of a flexible pipe with axially-varying structural parameters.

The dynamic behaviors of the pipes, considered as Euler or Timoshenko beam, with internal flow have been studied fine in history. Early in 1855, Brillouin observed the self-excited vibrations of cantilever pipes. The first published study of dynamic behaviors of the pipes with internal flow was given by Bourrières (Bourrières et al., 1939), where the equation of motion was obtained and analysed carefully to come to a famous conclusion of stability. Considering a pipe conveying fluid is not "closed" systems but "open" systems, Benjamin (Benjamin, 1961) studied a matter of pipe with internal flow via Lagrange method and obtained a formula that express energy transfer from fluid to pipe. By using this formula, the stability is divided into two kinds of stability. One is bucking instability; another is flutter instability. Holmes (Holmes, 1978) used a development of Liapunov's second method to prove that the pipes supported at both ends do not have the flutter instability. Gregory and

* Corresponding author. Institute of Mechanics, Chinese Academy of Sciences, Beijing, 100190, China.
E-mail address: wmchen@imech.ac.cn (W. Chen).
[1] These authors contributed equally to this work.

https://doi.org/10.1016/j.oceaneng.2021.108631
Received 1 September 2020; Received in revised form 15 November 2020; Accepted 10 January 2021
Available online 3 February 2021
0029-8018/© 2021 Elsevier Ltd. All rights reserved.

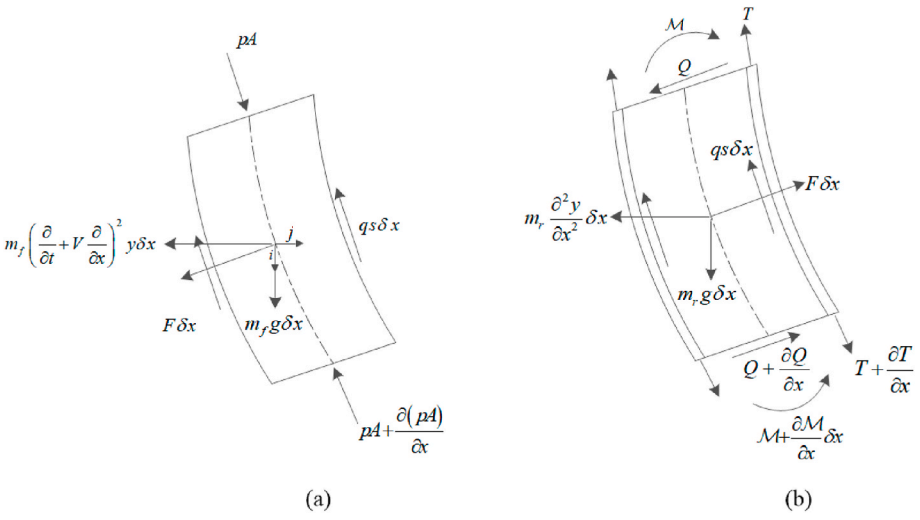

Fig. 1. (a) Fluid element and (b) Pipe element.

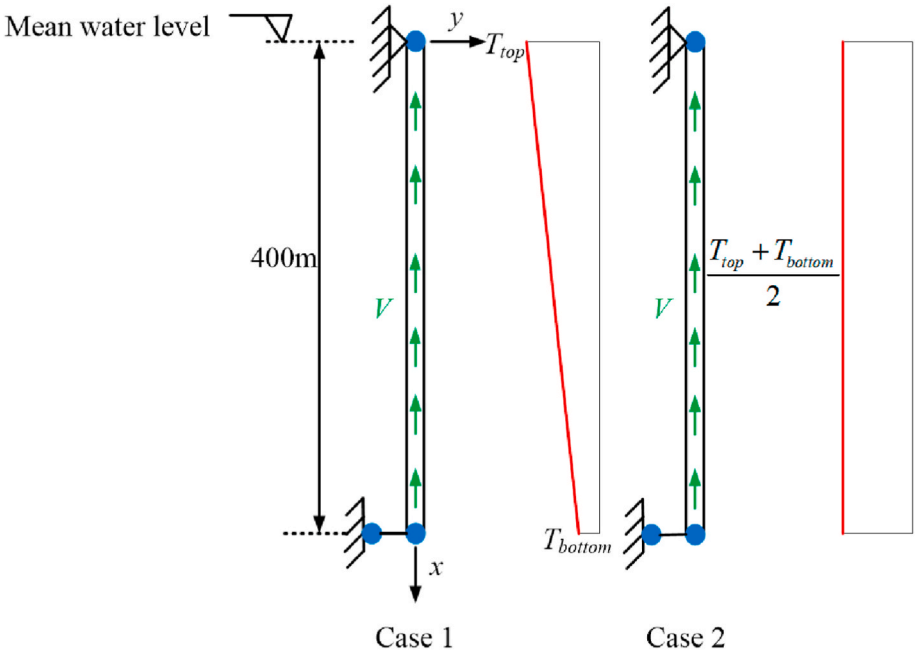

Fig. 2. Schematic of the pipe conveying fluid.

Table 1
Parameters of the pipe.

Appendix A. Parameter	Appendix B. Value
Outside diameter	205.0 mm
Inner diameter	150.0 mm
Length	400.0 m
Mass of pipe per unit length	30.0 kg/m
Tensile stiffness	1.536e9N
Mass of fluid per unit length	17.67 kg/m
Bending stiffness	6.19e5Nm^2
Pretension T_0	1, 0000.0 N

Table 2
Comparison of the pipe frequencies.

Appendix C. Dimensionless tension	Appendix D. Numerical	Appendix E. Theoretical	Appendix F. Differences (%)
0.00	9.870	9.870	0.000
0.20	8.829	8.828	0.015
0.40	7.648	7.645	0.037
0.60	6.247	6.242	0.068
0.80	4.423	4.414	0.163
0.90	3.132	3.121	0.353
0.95	2.223	2.207	0.731
1.00	0.273	0.000	

Païdoussis (Gregory and Païdoussis, 1966a, 1966b) established firstly the equation of motion by using the element body, then verified the flutter instability of cantilever pipe via theoretical and numerical calculations and experiment. Their work found a phenomenon that the system appears unstable, regain stability and instability again with increasing the velocity of fluid in some specific mass ratio. Païdoussis and Issid (Païdoussis. M P, Issid N T, 1974) established the motion equation of normal pipes with internal flow considering the effect of Kelvin-Voigt constitutive law, tension, and gravity, etc. They considered

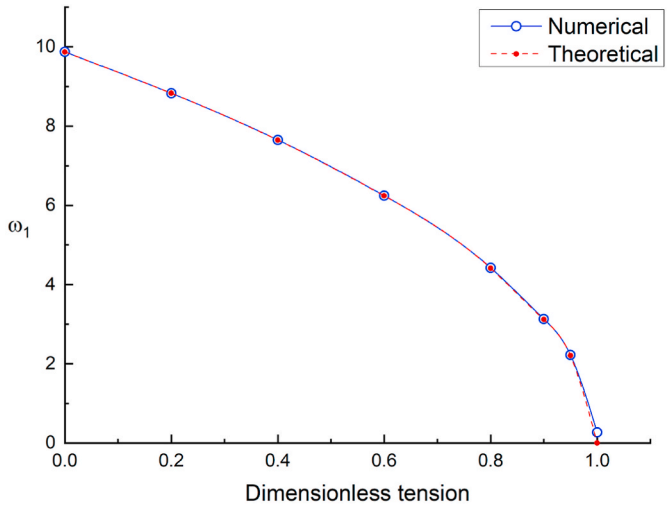

Fig. 3. Comparison of the numerical and theoretical results of the first-order frequency.

two cases of flow velocity that one was mean flow, the other was harmonically perturbed and obtained some conclusions that include the effect of viscous and viscoelastic dissipation diminish the extent of instability regions, etc. Païdoussis and Laithier (M, P, Païdoussis, et al., 1976) studied the vibration question of the pipes with internal flow by using Timoshenko beam model and the element body and they solved the equation of motion by using the variational method and the finite element method. It was found that the transverse shear effect reduces the eigenfrequencies and critical flow velocities of the cantilever pipe. Païdoussis and Laithier (Laithier, B. E., and M. P. Païdoussis, 1981) utilized two kinds of considerations to derive the equation of motion. One was to think of the system as an "open" system that exist open surface that can transport momentum, which corresponding to the modified Hamilton's principle; another was action of fluid that be viewed as external force, which corresponding to Hamilton's principle. Based on these two considerations, two kinds of Hamiltonian expressions of the Timoshenko beam for transportation fluid were established. Païdoussis, Luu and Laithier (Païdoussis. M P et al., 1986), for short pipe, used means of the Timeoshenko beam theory and refined fluid mechanics model that is based on potential flow theory to derive equation of motion. They obtained the non-dimensional critical velocity of a cantilever pipe as a function of the slenderness ratio by calculation and found that in contrast to plug-flow model, the eigenfrequencies and critical velocity increase for short pipes champed at both ends. The experimental results shown that refined fluid mechanics model is better than plug-flow theory. Pramila and Laukkanen (Pramila A et al., 1991) studied the pipes conveying fluid by using finite element method and Timoshenko beam element. The calculation results shown that a few elements are needed to obtain the critical velocities which is differ less than 1% from the ref (Païdoussis. M P et al., 1986). in undamped cases. Chen established the equation of motion of circular pipes by using Halmiton's principle in (Chen S S, 1972a) and the element body in (Chen S S, 1972b). The results shown that the critical velocity decrease with increasing total angle and the mechanism of instabilities is same as straight pipes in (Chen S S, 1972a). When there is no displacement at the end, the system is conservative system that subject to buckling-type instability. When the pipes are allowed to move at the ends, the system is non-conservative system that subject to buckling-type and flutter-type instability. Chen (Chen, S S, 1973) used Hamilton's principle to derive equation of space motion, which found that in-plane motion and out-of-plane motion is no coupling. Dai (Dai et al., 2013) studied fluid-conveying cantilevered pipe consisting of two segments made different materials by using the finite element method. For a hybrid pipe consisting of two segments with in identical lengths, it is easier to lose

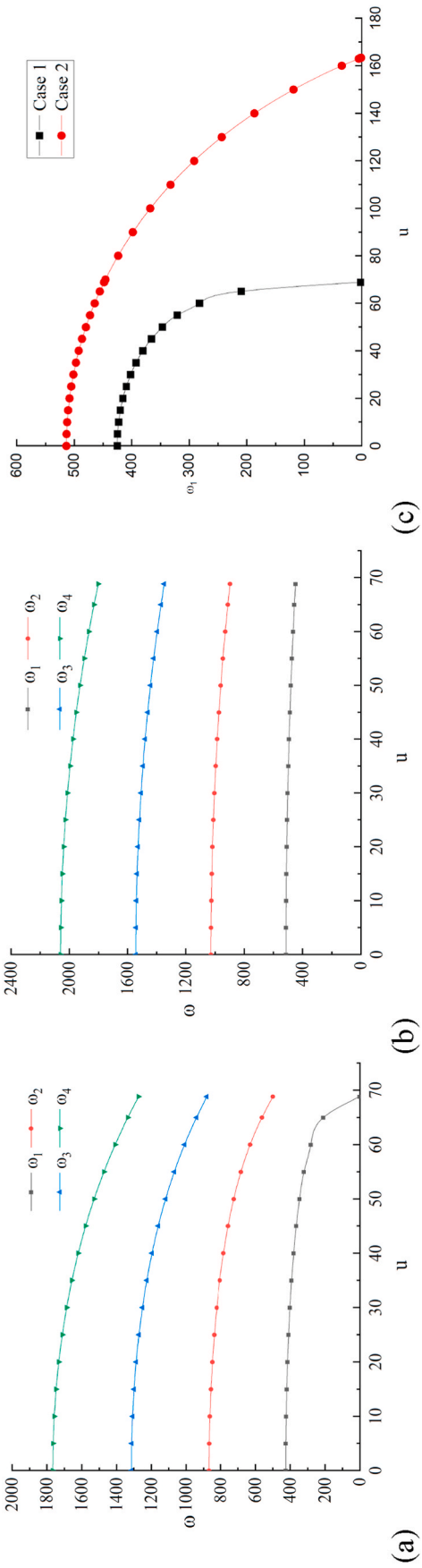

Fig. 4. Pipe frequency under dimensionless flow velocity*u*in range of 0–70 (a) Case 1 (b) Case 2 (c) Variation of the first frequency with flow velocity*u*in Case 1 and Case 2.

Table 3
Comparison of the pipe frequencies.

Appendix G. u	Appendix H. Case 1(ω)			Appendix I. Case 2(ω)		
	Mode 1	Mode 2	Mode 3	Mode 1	Mode 2	Mode 3
0	425.361	868.446	1314.352	513.537	1027.604	1542.729
5	424.744	867.300	1312.677	513.185	1026.898	1541.847
10	422.892	863.685	1307.563	512.215	1024.959	1538.849
15	419.806	857.600	1298.922	510.539	1021.696	1533.911
20	415.309	849.047	1286.665	508.247	1017.023	1527.033
25	409.313	837.673	1270.617	505.249	1011.027	1518.127
30	401.730	823.212	1250.337	501.545	1003.708	1507.194

stability for soft pipe segment at the clamped end than for hard pipe segment at clamped end. When two segments with in identical length, they calculated first four modes and found the flutter instability may occur in any of first four natural modes with the position or material of segment changed. When a material with greater stiffness is located at the fixed end, its characteristic frequency is greater than when the material with less stiffness is located at the fixed end. Meng (Meng et al., 2017) studied the dynamic behaviors of marine pipe undergoing both internal and external flow by using the Euler-Bernoulli beam theory and the finite element method. The critical internal flow velocity increases with the increase of internal flow velocity. When Montoya-Hernández (Montoya-Hernandez et al., 2014) studied the dynamic behaviors of multiphase flow with solid, liquid and gas in marine pipe transportation, multiphase flow model simplified to a homogenous model by using the weights method. Dai (Dai et al., 2014) derived the nonlinear dynamic equation of a pipe with both ends under the action of internal and external flow based on the Hamilton's principle and the Galerkin discretization. Reza(Reza Bahaadini, et,al. 2018) used the extended Galerkin approach to study a stability of a composite thin-walled cantilever pipe conveying fluid and supported at free end by linear translational and rotational springs. Geng(Geng Peng, et,al. 2018) investigated axial and transverse non-linear vibrations of a simply supported pipe conveying fluid by using the Galerkin's method. A pipe conveying fluid problem with a linear ramp distribution of the density along the pipe was studied by B.Giacobbi(B.Giacobbi, et al. 2020). The CFD-FEA simulations and the Galerkin's method were often adopted.

It is noted that most of the current researches focus on structures with axially-uniform properties. In practice, for a flexible pipe in deep water, its structure parameter, e.g. axial tension, is no longer uniform along pipe length. And, by now, few reports have been seen on dynamic response, rather than stability problem, of a pipe with internal flow. In this study, the dynamic characteristics, i.e. the natural modal shape and frequency along with the dynamic response of a pipe with axially-varying tension are examined. As a comparison, the results of a simplified model, a uniform pipe, are also calculated. Our numerical results show that the dynamic behaviors, i.e. the modal shapes and dynamic responses, are significantly different from the pipe with uniform tension.

2. Models

2.1. Governing equation

The equation of motion of a vertical pipe conveying fluid is derived by using the element body and the Newton's second law.

For the fluid element in Fig. 1(a), we can obtain the equilibrium equation by using the Newton's second law:

$$-A\frac{\partial p}{\partial x} - qs + m_f g + F\frac{\partial y}{\partial x} = 0 \tag{1}$$

$$F + A\frac{\partial}{\partial x}\left(p\frac{\partial y}{\partial x}\right) + qs\frac{\partial y}{\partial x} + m_f\left(\frac{\partial}{\partial t} + V\frac{\partial}{\partial x}\right)^2 y = 0 \tag{2}$$

where y is the transverse displacement, V is the flow velocity, $q$is the shear stress on the internal surface of the pipe, s is the inner perimeter of the pipe, and m_f is the mass of the internal fluid per unit length. Similarly, for the pipe element (Fig. 1(b)) we have

$$\frac{\partial T}{\partial x} + qs + m_P g - F\frac{\partial y}{\partial x} = 0 \tag{3}$$

$$\frac{\partial Q}{\partial x} + F + \frac{\partial}{\partial x}\left(T\frac{\partial y}{\partial x}\right) + qs\frac{\partial y}{\partial x} - m_P\frac{\partial^2 y}{\partial x^2} = 0 \tag{4}$$

$$Q = -\frac{\partial \mathcal{M}}{\partial x} = -EI\frac{\partial^3 y}{\partial x^3} \tag{5}$$

where $F$is the transverse force per unit length between pipe wall and fluid, $\mathcal{M}$ is the bending moment, $EI$is the bending stiffness, and $m_p$is the mass of pipe per unit length. Then we can get the governing equation of fluid-solid dynamics of a vertical pipe conveying fluid as

$$EI\frac{\partial^4 y}{\partial x^4} + \left[m_f V^2 - \left(m_f + m_p\right)g(L-x)\right]\frac{\partial^2 y}{\partial x^2} + 2m_f V\frac{\partial^2 y}{\partial x \partial t} + \left(m_f + m_p\right)g\frac{\partial y}{\partial x} + \left(m_f + m_p\right)\frac{\partial^2 y}{\partial t^2} = 0 \tag{6}$$

where g is the gravitational acceleration. By comparison with the equation of motion of a beam with variable tension:

$$EI\frac{\partial^4 y}{\partial x^4} + \frac{\partial}{\partial x}\left(T(x)\frac{\partial y}{\partial x}\right) + m_p\frac{\partial^2 y}{\partial t^2} = 0 \tag{7}$$

Here, the second and the fourth term on the left side of Eq. (1), which essentially describe the effect of fluid centrifugal force and fluid-&structure gravity respectively, can be expressed in terms of a axially-varying tension as follow

$$T(x) = m_f V^2 - \left(m_f + m_p\right)g(L-x) \tag{8}$$

where $T(x)$ represents a compressive effect when it is plus, while it represents tension effect when it is minus. We can see that the axial tension $T(x)$ is linearly-varying along the pipe length as shown in Fig. 2.

Defining the dimensionless quantities:

$$\xi = \frac{x}{L}, \eta = \frac{y}{L}, \tau = \left(\frac{EI}{m_f + m_p}\right)^{\frac{1}{2}}\frac{t}{L^2}, u = \left(\frac{m_f}{EI}\right)^{\frac{1}{2}}LV, \beta = \frac{m_f}{m_f + m_p},$$

$$\gamma = \frac{\left(m_f + m_p\right)L^3}{EI}, \zeta = \frac{TL^2}{\pi^2 EI} \tag{9}$$

Equation (6) can be rewritten in the dimensionless form:

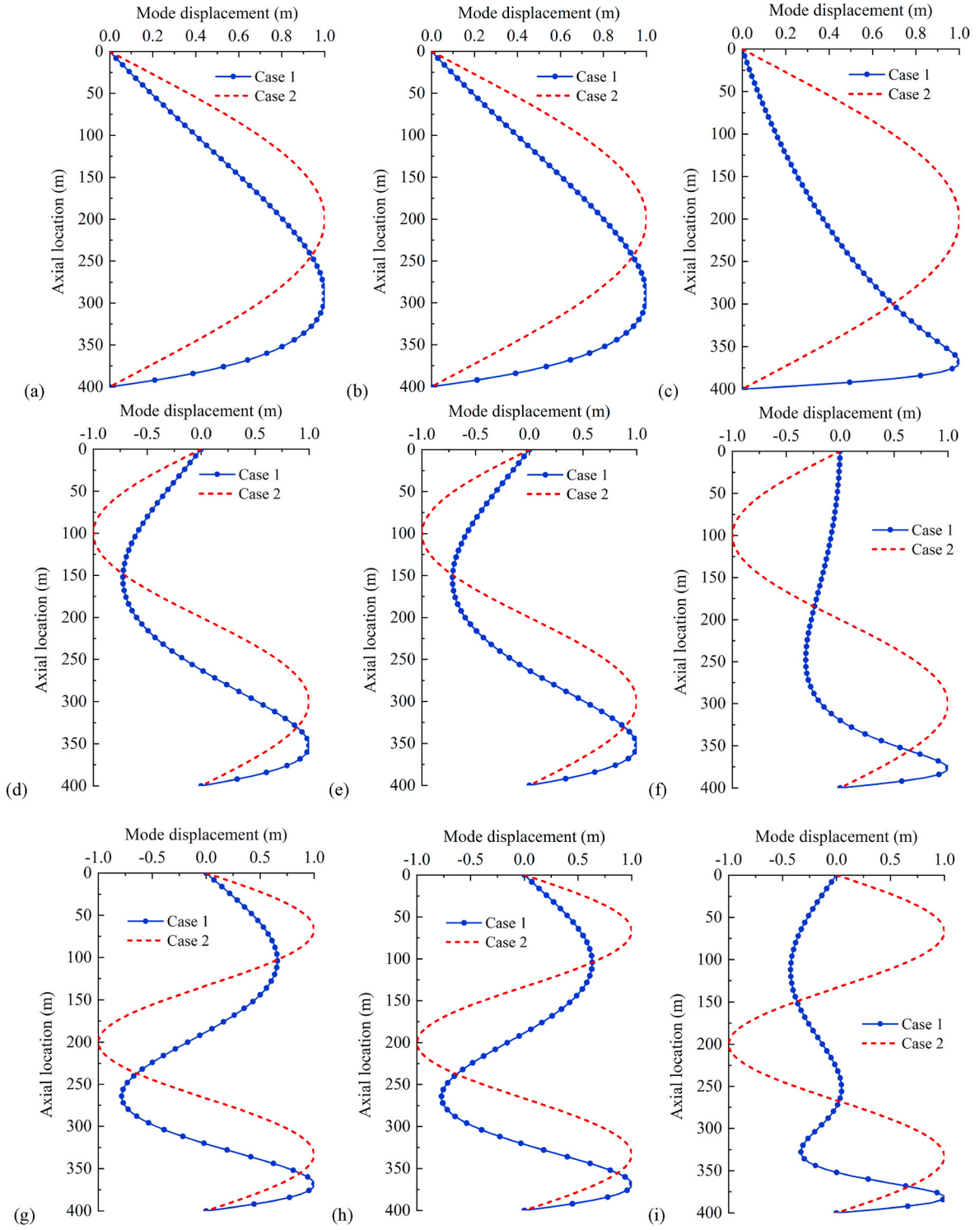

Fig. 5. Comparison of the first three modal shapes (a) the first mode at $u = 0$ (b) the first mode at $u = 10$ (c) the first mode at $u = 64$ (d) the second mode at $u = 0$ (e) the second mode at $u = 10$ (f) the second mode at $u = 64$ (g) the third mode at $u = 0$ (h) the third mode at $u = 10$ (i) the third mode at $u = 64$.

$$\frac{\partial^4\eta}{\partial\xi^4}+\left[u^2-\gamma(1-\xi)\right]\frac{\partial^2\eta}{\partial\xi^2}+2\beta^{\frac{1}{2}}u\frac{\partial^2\eta}{\partial\xi\partial\tau}+\gamma\frac{\partial\eta}{\partial\xi}+\frac{\partial^2\eta}{\partial\tau^2}=0 \tag{10}$$

Regarding the motion of the pipe is a periodic vibration, motions of the form $\eta = Y(\xi)e^{i\omega\tau}$ are considered. The dimensionless frequency ω can be expressed by the dimensional radian frequency Ω as

$$\omega=\left(\frac{m_f+m_p}{EI}\right)^{\frac{1}{2}}L^2\Omega \tag{11}$$

2.2. FEM approach

The pipe is uniformly divided into n two-node Euler beam elements. For representativeness and simplicity, only the translation displacements in x-y plane $[u_i, v_i]$ and one rotation degree $\theta_i$around $z$axis, of per node, are considered. Then the governing equation of the pipe with many DOFs (degrees of freedom) can be written as follow:

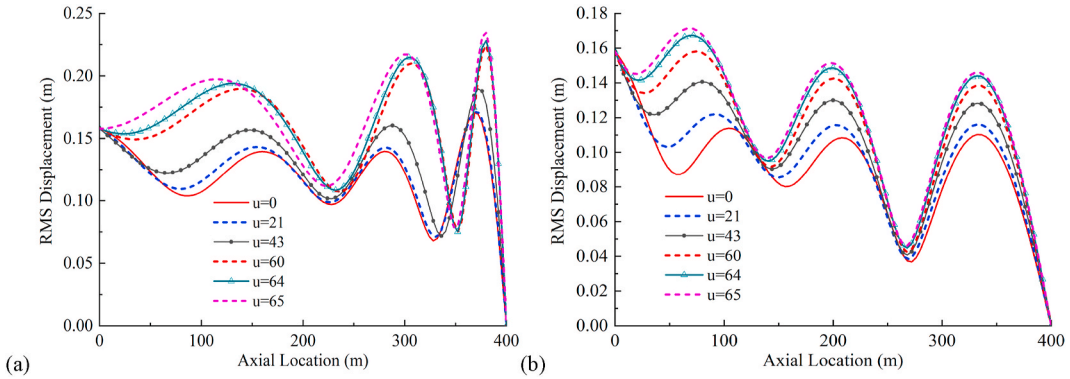

Fig. 6. The RMS curve of pipe displacement at u = 0, 21, 43, 60, 64 and 65 (a) Case 1 (b) Case 2.

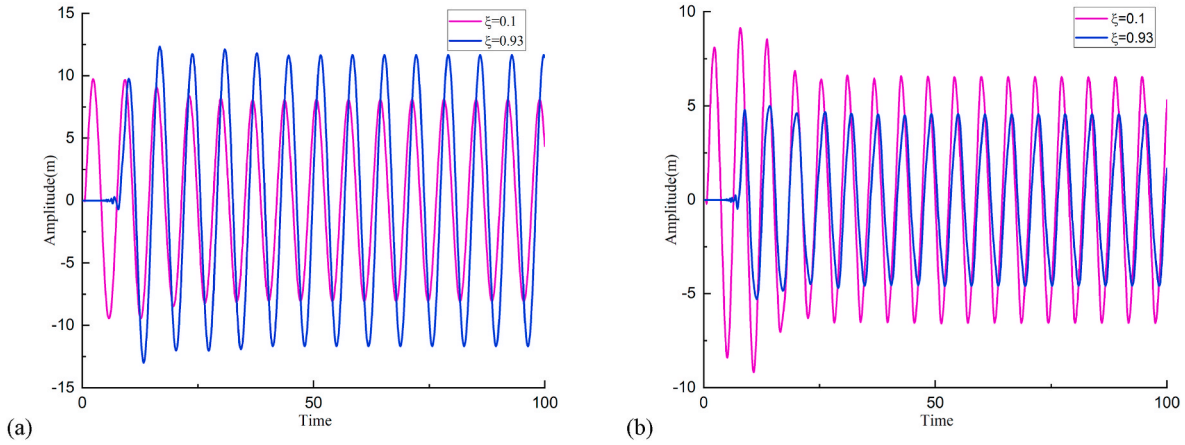

Fig. 7. The response of pipe displacement with dimensionless parameterξ = 0.1 and 0.93 at u = 10 (a) Case 1 (b) Case 2.

$$M\ddot{U} + C\dot{U} + KU = 0 \tag{12}$$

where M is the mass matrix including the fluid mass and the structure mass, C is the damping matrix considering the interaction between fluid and structure, and $K$is the stiffness matrix. $U$is the displacement vector. The displacement vector of the beam element is:

$$U_i = [u_i, v_i, \theta_i, u_{i+1}, v_{i+1}, \theta_{i+1}], i = 1, \ldots, n \tag{13}$$

In Eq. (1), the third term of the left-side represents the Coriolis force which is usually considered as damping effect to system. The damping matrix of the element is calculated as follows:

$$C_e = 2m_f V \cdot N^T \cdot \frac{\partial N}{\partial x} \tag{14}$$

where N is the shape function matrix of the beam element, and the damping matrix C of the whole structure can be obtained by assembling the damping matrix C_e of all elements.

To solve governing equation (12) of the pipe, an in-house code was implemented (Laithier and Païdoussis, 1981; Guo et al., 2018; Li et al., 2020), and the Newmark method is employed here to adjust the distribution of the structural acceleration and velocity in the code. The interpolation functions of the displacement and acceleration are written as:

$$\begin{aligned} \dot{U}_{t+\Delta t} &= \dot{U}_t + \left[(1-\phi)\ddot{U}_t + \phi\ddot{U}_{t+\Delta t}\right]\Delta t \\ U_{t+\Delta t} &= U_t + \dot{U}_t\Delta t + \left[\left(\frac{1}{2} - \alpha\right)\ddot{U}_t + \alpha\ddot{U}_{t+\Delta t}\right]\Delta t^2 \end{aligned} \tag{15}$$

2.3. Model parameters

In this study the dynamic characteristics, i.e. the natural modal shape and frequency along with the dynamic response of a vertical pipe with axially-varying tension, are examined under different internal flow velocities. The results of the simplified model (pipe with uniform tension) are also calculated as a comparison. The two analysed models, with different axial tension conditions, are shown in Fig. 1. T_{top} represents the top tension and T_{bottom} represents the bottom tension. The pipes are simply supported at top and bottom ends, and its main structural and fluid parameters are presented in Table 1.

Regarding the axial tension of the vertical pipe, one is composed of pre-tension T_0 and the other is tension caused by the structural gravity. In Case 1, the actual gravity distribution along pipe length is considered, and the axial tension component caused by the pipe gravity gradually decreases along the length (x-axis direction) of the pipe, as shown in Eq. (8). In Case 2, as a simplified model, the part of the axial tension caused by the gravity is assumed as a uniform tension, which equal to the average value the structural gravity, i.e.0.5G And, $G$is the gravity of the pipe (including internal flow, $G = (m_f + m_p)gL$).

3. Numerical results and discussions

The dynamic characteristics of a vertical pipe with different internal flow velocities are calculated through our model and the influence of the axially-varying tension on the modal shape of the pipe will be analysed. Furthermore, the responses of the vertical pipe caused by the periodic motion of the top-end point are presented and the influences of the flow velocity and axial tension variation on the displacement response and its temporal-spatial evolution of the pipe will be studied.

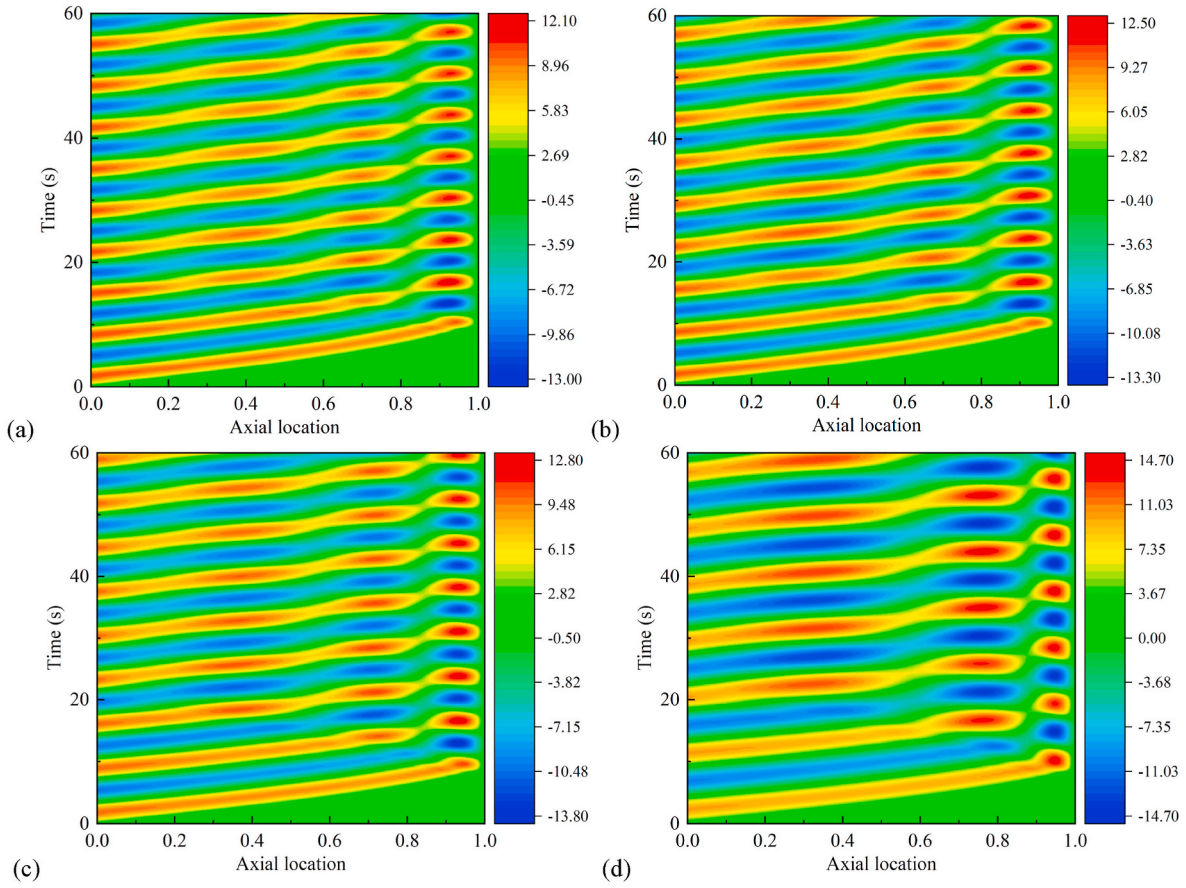

Fig. 8. Temporal-spatial evolution of riser displacement for Case 1 (a) $u = 0$ (b) $u = 10$ (c) $u = 43$(d) $u = 64$.

3.1. Model verification

To verify our numerical model, the first-order frequencies of the pipe under different axial compressive force are calculated and compared with the theoretical results. The pipe frequencies are shown in Table 2 and Fig. 3. The velocities and frequencies are all dimensionless. It can be seen that the calculated frequencies agree well with the theoretical ones (the difference is less than 1.0%).

3.2. Inherent dynamic characteristics

Fig. 4 shows the plots of the natural frequency versus the internal flow velocity. It is seen that, owing to the axially-varying tension, the frequency becomes smaller than the pipe with uniform tension, e.g. by 20.7% and 18.7% for the first two frequencies as $u = 0$. The frequency difference increases with increasing flow velocity. With the increase of the internal flow velocity, the frequency gradually decreases. And the first-order frequency drops very close to zero, or the pipe losses its stability when the dimensionless velocity u approaches to about 68. But the frequencies of the uniform axial tension model do not change obviously, see Table 3. This is mainly because that, with increasing flow velocity, the tension at the bottom end of the pipe in Case 1 becomes much smaller than in Case 2. In other words, the critical velocity of the pipe with axially-varying tension gets smaller, that should be paid careful attention during stability analysis of a pipe in deep water.

The comparisons of the first three modal shapes, at different flow velocities, are shown in Fig. 5. Interestingly, the modal shape is no longer symmetric/anti-symmetric about the midpoint of the pipe. In other words, the modal wave length gets smaller while the wave amplitude gets larger, owing to the axially-varying tension. And, the maximum modal amplitude moves toward the position with smaller axial tension.

3.3. Dynamic responses

In this section, the dynamic response of the pipe caused by top-end motion is analysed at different flow velocities. The top-end frequency is selected as the 3rd bending frequency of the pipe, and the motion amplitude is 10 m.

For the pipe with axially-varying tension, the root mean square (RMS) of displacements under different internal flow velocities is presented in Fig. 6(a). It can be seen that with the increase of velocity, the displacement response of the pipe increases gradually, because the axial compression caused by internal flow results in a decrease of the pipe stiffness. In addition, it can be seen that the maximum displacement occurs near the area close to the bottom-end where the tension is smaller, which lead to the curvature of bottom-end to be larger than in Case 2. Therefore, we may say if simplified model in Case 2 is used to simulate a pipe with axially-varying tension, it will underestimate the bending moment at the pipe bottom and increase the risk of structure safety in practice. And, owing to the decreasing tension, the displacement response of the top-end could be amplified during its propagating along pipe length. However, as shown in Fig. 6(b), the displacement response of the top-end is reduced during its propagating along pipe length. This is mainly due to the Coriolis force, which is corresponding to damping effect.

As a comparison, the response of the pipe under uniform axial tension is shown in Fig. 7(b). On the contrary, the response of the pipe with uniform axial tension gradually decreases along the length of the pipe.

Considering axially-varying tension, the temporal and spatial

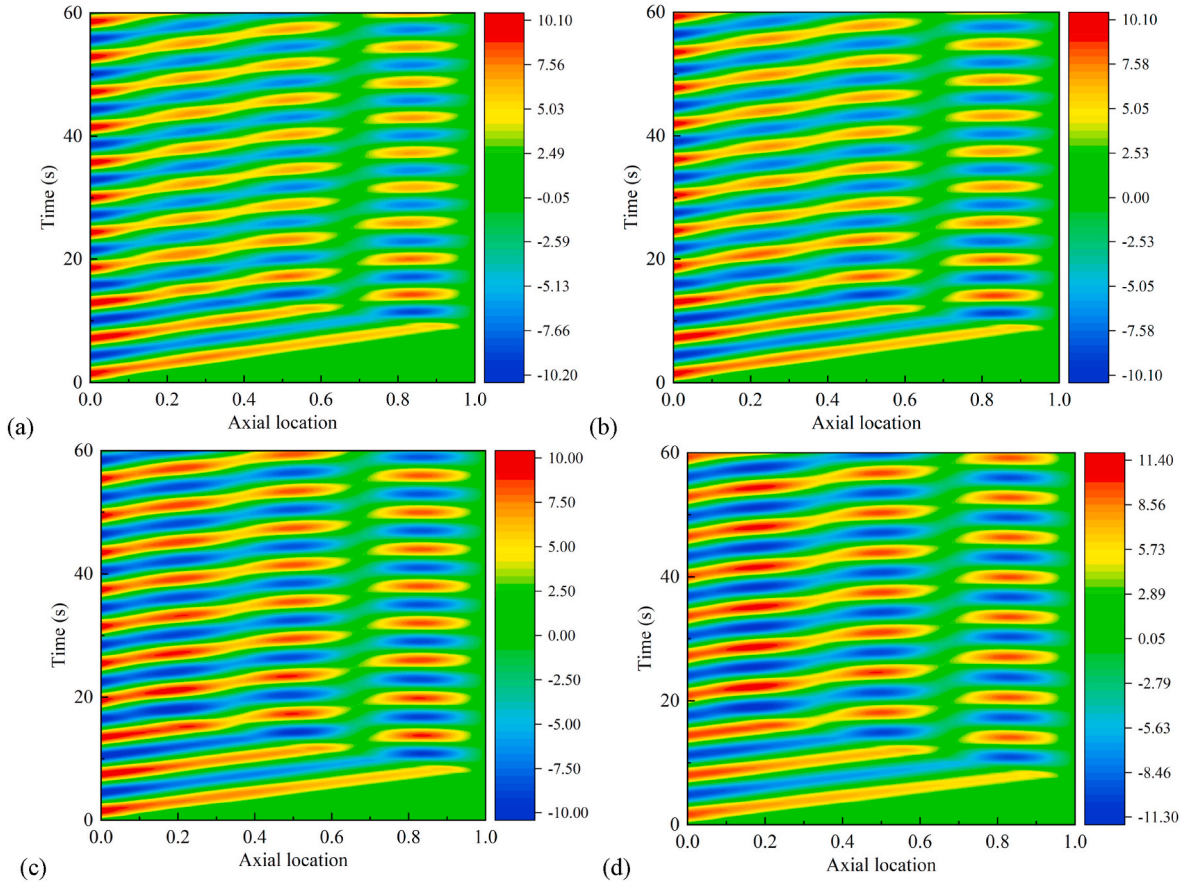

Fig. 9. Temporal-spatial evolution of riser displacement for Case 2 (a) $u = 0$ (b) $u = 10$ (c) $u = 43$(d) $u = 64$.

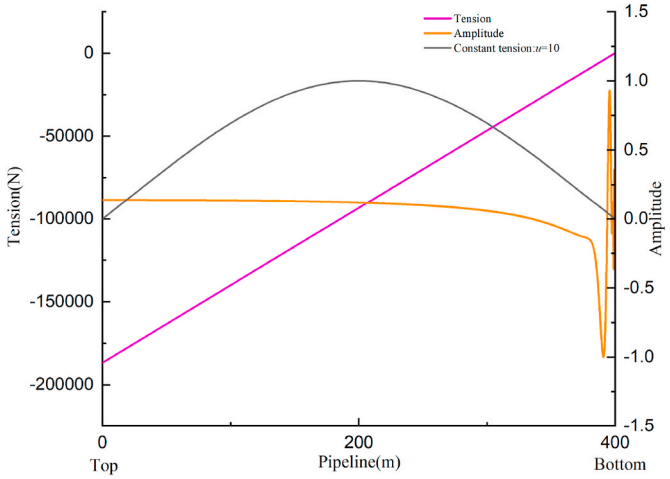

Fig. 10. Modal shapes and tension along the pipeline.

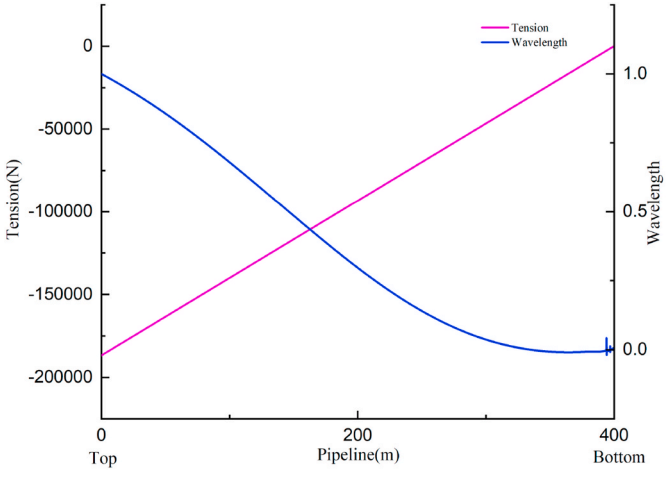

Fig. 11. Wavelength changes along the pipeline.

evolutions of the pipe displacement are presented in Fig. 8. Obvious wave propagation characteristics can be seen in Fig. 8. Generally, there exists three standing waves over the whole length, and the wavelength gets significantly smaller during propagation along the pipe length. With the increase of internal flow velocity, the wavelength of the first standing wave increases, and the peak position of the third wave moves down to the bottom-end. This phenomenon is consistent with the RMS result shown in Fig. 6(a).

As a comparison, the wavelength and peak position have no obvious change for case of the pipe with uniform tension, as shown in Fig. 9. It is also noted that the displacement amplitude is larger, up to 19.7%, than the uniform tension pipe owing to the axially-varying tension.

3.4. Discussions

To theoretically explain the changes of the amplitude and wavelength along the axis, firstly, we consider the case of constant tension, namely$T = m_f V^2$. The governing equation is

$$EI\frac{\partial^4 y}{\partial x^4} + m_f V^2 \frac{\partial^2 y}{\partial x^2} + 2m_f V \frac{\partial^2 y}{\partial x \partial t} + \left(m_f + m_p\right)\frac{\partial^2 y}{\partial t^2} = 0 \tag{16}$$

Assuming the solution of Eq. (16) is$y = e^{i(kx-\Omega t)}$, $k$is wave number and $\Omega$is frequency. Substitute $y = e^{i(kx-\Omega t)}$[fx] into Eq. (16), the dispersion equation can be got as

$$EIk^4 - m_f V^2 k^2 + 2m_f Vk\Omega - (m_f + m_p)\Omega^2 = 0 \tag{17}$$

In general, the solution $k$of Eq. (17) is a function of Ω, then we can solve the Ω by using the boundary conditions. Here, we firstly solve the Ω by using finite element method and then substitute the Ω into Eq. (17). Accordingly, the solution of Eq. (16) can be got and k_1, k_2, k_3 and k_4 are obtained by solving Eq. (17). The general solution is

$$y = \alpha_1 e^{i(k_1 x-\Omega t)} + \alpha_2 e^{i(k_2 x-\Omega t)} + \alpha_3 e^{i(k_3 x-\Omega t)} + \alpha_4 e^{i(k_4 x-\Omega t)} \tag{18}$$

whereα_1, α_2, α_3 and α_4 are constant. The boundary conditions are

$$\begin{cases} y(0,t) = 0 \\ y(L,t) = 0 \end{cases} \quad \begin{cases} y''(0,t) = 0 \\ y''(L,t) = 0 \end{cases} \tag{19}$$

The prime represents the derivative with respect to x. Substitute (18) into (19), we can obtain

$$\begin{cases} \alpha_1 + \alpha_2 + \alpha_3 + \alpha_4 = 0 \\ k_1^2\alpha_1 + k_2^2\alpha_2 + k_3^2\alpha_3 + k_4^2\alpha_4 = 0 \\ e^{ik_1 L}\alpha_1 + e^{ik_2 L}\alpha_2 + e^{ik_3 L}\alpha_3 + e^{ik_4 L}\alpha_4 = 0 \\ k_1^2 e^{ik_1 L}\alpha_1 + k_2^2 e^{ik_2 L}\alpha_2 + k_3^2 e^{ik_3 L}\alpha_3 + k_4^2 e^{ik_4 L}\alpha_4 = 0 \end{cases} \tag{20}$$

Simplifying Eq. (20), we get

$$y = \left(Ae^{ik_1 x} + Be^{ik_2 x} + Ce^{ik_3 x} + e^{ik_4 x}\right)\alpha_4 e^{-i\Omega t} \tag{21}$$

$$\begin{cases} A = \dfrac{(k_2^2-k_1^2)(k_3^2-k_4^2)e^{ik_2 L} + (k_3^2-k_1^2)(k_4^2-k_2^2)e^{ik_3 L} + (k_4^2-k_1^2)(k_2^2-k_3^2)e^{ik_4 L}}{(k_2^2-k_1^2)(k_3^2-k_1^2)(e^{ik_3 L}-e^{ik_2 L})} \\ B = \dfrac{(k_4^2-k_1^2)(e^{ik_4 L}-e^{ik_3 L})}{(k_2^2-k_1^2)(e^{ik_3 L}-e^{ik_2 L})} \\ C = \dfrac{(k_4^2-k_1^2)(e^{ik_4 L}-e^{ik_2 L})}{(k_3^2-k_1^2)(e^{ik_3 L}-e^{ik_2 L})} \end{cases} \tag{22}$$

So the function of modal shape $Y(x)$can be written as

$$Y(x) = \mathrm{Re}\left(Ae^{ik_1 x} + Be^{ik_2 x} + Ce^{ik_3 x} + e^{ik_4 x}\right) \tag{23}$$

Because we only consider the variation of modal shape along the axis, α_4 is neglectable. For the case of variable tension, replacing$T = m_f V^2$ with $T(x) = m_f V^2 - (m_f + m_p)g(L - x)$. When the dimensionless velocity u is 10, we can get the variation of modal shape along the axis as shown in Fig. 10.

Fig. 10 shows that the amplitude of each point on the beam increases along the axial direction as the tension decreases from the top end to bottom end. The axial force changes from tension to compressive force when it is closer to the bottom end, which cause the amplitude of the points on the bottom of the beam increases sharply.

As for wavelength changes along the pipe length, we firstly consider the case that T' is infinitesimal. If the tension is constant, the amplitude and wavelength is constant. Accordingly, we can assume that the variation of amplitude of modal shape and wavelength is infinitesimal whenT' is infinitesimal. Based on this assumption, the WKB solution is employed.

The Wentzel-Kramers-Brillouin (WKB) approximation method is used to obtain the approximate solution of the one-dimensional stationary Schrödinger equation. It is assumed that a particle with energy E passes through the region of potential energy $V(x)$, where $V(x)$ is a constant, when $E > V$, the form of the wave function is:

$$\psi(x) = Ae^{\pm ikx}, k = \sqrt{2m(E-V)/\hbar} \tag{24}$$

A being positive means the particle moves to the right, while negative means it moves to the left. The wave function is an oscillating function, with a fixed wavelength ($\lambda = 2\pi/k$) and a constant amplitude A. If $V(x)$ is not a constant, but the change is very slow compared to λ, Consequently, in the regions that contain many full-wavelength, potential energy can be considered basically constant. In this way, in addition to the slow change of wavelength and amplitude with x, it is reasonable to think that ψ actually still maintains a sinusoidal form. That is, one can assume:

$$\psi(x) = A(x)e^{\pm i\phi(x)} \tag{25}$$

The governing equation is

$$EI\frac{\partial^4 y}{\partial x^4} + \frac{\partial}{\partial x}\left(T\frac{\partial y}{\partial x}\right) + 2m_f V\frac{\partial^2 y}{\partial x \partial t} + (m_f + m_p)\frac{\partial^2 y}{\partial t^2} = 0 \tag{26}$$

Assuming the solution of Eq. (24) is

$$y = Y(x)e^{i\Omega t}, Y(x) = a(x)e^{i\theta(x)} \tag{27}$$

and

$$\frac{d\theta(x)}{dx} = k(x) = \frac{2\pi}{\lambda(x)} \tag{28}$$

where $a(x)$, $k(x)$ and $\lambda(x)$ are amplitude of modal shape, wave number and wavelength, respectively. Substituting Eq. (27) and Eq. (28) into Eq. (26) and neglecting infinitesimal, we can obtain the equation as

$$EI\left(k^4 a - 6ik'k^2 a - 4ik^3 a'\right) + T\left(ik'a - k^2 a + 2ika'\right) + T'(ika + a')$$

$$- 2m_f V^2 \Omega i(ika + a') - (m_f + m_p)\Omega^2 a = 0 \tag{29}$$

Neglecting the infinitesimal terms, the dispersion equation can be written as

$$EIk^4 - Tk^2 + 2m_f Vk\Omega - (m_f + m_p)\Omega^2 = 0 \tag{30}$$

Substituting Eq. (30) into Eq. (29), Eq. (29) can be simplified to the following form

$$a\left(-6EIik'k^2 + iTk' + iT'k\right) + 2a'\left(-2EIik^3 + ikT + \frac{1}{2}T' - m_f V\Omega i\right) = 0 \tag{31}$$

Multiplying both sides of Eq. (31) by $a(x)$ and considering that the tension T varies linearly along the axis, Eq. (31) is transformed into following form

$$\left(2EIk^3 - kT + m_f V\Omega + \frac{1}{2}T'i\right)a^2 = constant \tag{32}$$

When velocity of flow is small, the frequency ω is a real number. Retaining the real part of Eq. (32), we have

$$(2EIk^3 - kT + m_f V\Omega)a^2 = constant \tag{33}$$

It is noted that when T' is not infinitesimal, Eq. (33) still may be used to qualitatively explain the relationship between tension and wavelength. Combining Eq. (23) and Eq. (33), the relationship between tension and wavelength can be shown in Fig. 11, which dimensionless velocity u is 10. The figure shows that the wavelength decreases when the tension decreases along the axial direction. The small fluctuation in the curve at the bottom end is mainly due to the numerical calculation, where the value of wave length is very close to zero.

4. Conclusions

In this study the dynamic characteristics, stability and response of a fluid conveying pipe, under consideration of non-uniform axial tension, are examined through our FEM numerical simulations. The influences of axially-varying tension on the frequency, modal shape and dynamic

response are presented. Our numerical results show that:

31. The non-uniform tension has significant impacts on the dynamic characteristics and response of the pipe. Owing to the axially-varying tension, the frequency is smaller than the pipe with uniform tension, e.g. by 20.7% and 18.7% for the first two frequencies as $u = 0$. The modal wave length gets smaller while the wave amplitude gets larger, and the maximum modal amplitude moves toward the position with smaller axial tension. The critical velocity of the pipe with axially-varying tension gets smaller, that should be paid careful attention during stability analysis of a pipe in deep water. The displacement response of the top-end could be amplified during its propagating along pipe length. The maximum displacement occurs near the area close to the bottom-end, and the displacement amplitude is larger, up to 19.7%, than the uniform tension model.

CRediT authorship contribution statement

Dingbang Yan: formulations derivations, theoretical analysis, Writing – original draft. **Shuangxi Guo:** FEM numerical analysis, Visualization, Writing – original draft. **Yilun Li:** FEM validations, Writing – original draft. **Jixiang Song:** assistant work of numerical analysis and validation. **Min Li:** Supervision, of FEM models developments and reviewing on analysis. **Weimin Chen:** Conceptualization, Writing – review & editing, Supervision.

Declaration of competing interest

The authors declare that they have no known competing financial interests or personal relationships that could have appeared to influence the work reported in this paper.

Acknowledgements

The authors of this paper would like to thank the financial supports provided by the Strategic Priority Research Programme of the Chinese Academy of Sciences (Grant No. XDA22000000).

References

Bahaadini, Reza, Reza Dashtbayazi, Mohammad, Hosseini, Mohammad, Khalili-Parizi, Zahra, 2018. Stability analysis of composite thin-walled pipes conveying fluid. Ocean Eng. 160, 311–323.

Benjamin, T.B., 1961. Dynamics of a system of articulated pipes conveying fluid. I. Theory[J]. Proc. Roy. Soc. Lond. Math. Phys. Sci. 261 (1307), 457–486.

Bourrières, François-Joseph, Bénard, Henri, 1939. Sur un phénomène d'oscillation auto-entretenue en mécanique des fluides reels. Publications Scientifiques et Techniques du M inistère de l'Air,No.147.

Chen, S.S., 1972a. Vibration and stability of a uniformly curved tube conveying fluid[J]. J. Acoust. Soc. Am. 51 (1B), 1087.

Chen, S.S., 1972b. Flow-induced in-plane instabilities of curved pipes[J]. Nucl. Eng. Des. 23 (1), 29–38.

Chen, S.S., 1973. Out-of-Plane vibration and stability of curved tubes conveying fluid[J]. J. Appl. Mech. 40 (2), 362.

Dai, H.L., Wang, L., Ni, Q., 2013. Dynamics of a fluid-conveying pipe composed of two different materials[J]. Int. J. Eng. Sci. 73 (Complete), 67–76.

Dai, H.L., Abdelkefi, A., Wang, L., 2014. Modeling and nonlinear dynamics of fluid-conveying pipes under hybrid excitations[J]. Int. J. Eng. Sci. 81, 1–14.

Geng, Peng, Xiong, Youming, Gao, Yun, Liu, Liming, Wang, Menghao, Zhang, Zheng, 2018. Non-linear dynamics of a simply supported fluid-conveying pipe subjected to motion-limiting constraints: two-dimensional analysis. J. Sound Vib. 435, 192–204.

Giacobbi, Dana B., Semler, Christian, Michael, P., Paidoussis, 2020. Dynamics of pipes conveying fluid of axially varying density. J. Sound Vib. 473, 10.

Gregory, R.W., Païdoussis, M.P., 1966a. Unstable oscillation of tubular cantilevers conveying fluid. I. Theory[J]. Proc. Roy. Soc. Lond. 293 (1435), 512–527.

Gregory, R.W., Païdoussis, M.P., 1966b. Unstable oscillation of tubular cantilevers conveying fluid. II. Experiments[J]. Proc. Roy. Soc. Lond. Math. Phys. Sci. 293 (1435), 528–542.

Guo, S., Li, Y., Li, M., et al., 2018. Dynamic Response Analysis on Flexible Pipe with Different Configurations in Deep-Water Based on FEM Simulation[C], ASME 2018, International Conference on Ocean, Offshore and Arctic Engineering.

Holmes, P.J., 1978. Pipes supported at both ends cannot flutter[J]. J. Appl. Mech. 45 (3), 619.

Laithier, B.E., Païdoussis, M.P., 1981. The equations of motion of initially stressed Timoshenko tubular beams conveying fluid[J]. J. Sound Vib. 79 (2), 175–195.

Li, Y., Guo, S., Chen, W., et al., 2020. Analysis on restoring stiffness and its hysteresis behavior of slender catenary mooring-line[J]. Ocean Eng. 209, 107521.

Meng, S., Kajiwara, H., Zhang, W., 2017. Internal flow effect on the cross-flow vortex-induced vibration of a cantilevered pipe discharging fluid[J]. Ocean Eng. 137, 120–128.

Montoya-Hernandez, D.J., Vazquez-Hernandez, A.O., Cuamatzi, R., et al., 2014. Natural frequency analysis of a marine pipe considering multiphase internal flow behavior [J]. Ocean Eng. 92, 103–113.

Païdoussis P., M., et al., 1976. Dynamics of Timoshenko beams conveying fluid[J]. J. Mech. Eng. Sci. 18 (4), 210–220.

Païdoussis, M.P., Issid, N.T., 1974. Dynamic stability of pipes conveying fluid[J]. J. Sound Vib. 33 (3), 267–294.

Païdoussis, M.P., Luu, T.P., Laithier, B.E., 1986. Dynamics of finite-length tubular beams conveying fluid[J]. J. Sound Vib. 106 (2), 311–331.

Pramila, A., Laukkanen, J., Liukkonen, S., 1991. Dynamics and stability of short fluid-conveying Timoshenko element pipes[J]. J. Sound Vib. 144 (3), 421–425.